Supporting information

A flexible concentric coupled re-entrant-star composite structure with an enhanced negative Poisson's ratio and mechanical strength

Mengting Zhao[b], Junli Chen[a, *], Xiaojing Wen[a], Bingqi Tian[a]

[a] School of Aeronautics, Shanghai Dianji University, Shanghai 201306, China.

[b] School of Mechanical Engineering, Shanghai Dianji University, Shanghai 201306, China.

* Corresponding author:

Junli Chen

School of Aeronautics, Shanghai Dianji University, Shanghai, 201306, China.

Email: chenjl@sdju.edu.cn

S1. List of Symbols

S2. Geometric derivations of unit cells

S3. Fabrication Procedure of NPR Metamaterials

S4. Cyclic loading testing

S5. Definition and Measurement of Poisson's Ratio

S6. Deformation mechanisms of RH and SH structures

S7. Definition and Calculation of the Effective Tangent Modulus and initial Modulus

S8. Statistical validation of tensile performance of CCRS, RH, and SH structures

S1. List of Symbols

Table S1. List of Symbols

Symbol	Description
l_R	Horizontal short-side length of the RH
l_{R1}	Diagonal rod length of the RH
l_{R2}	Horizontal rod length connecting the re-entrant angles of the RH
l_{S1}	Diagonal rod length of the SH
l_{S2}	Horizontal connecting rod length of the SH
l_{S3}	Vertical connecting rod length of the SH
l_{RS}	Horizontal rod length of the outer RH unit in CCRS
l_{RS1}	Diagonal rod length of the outer RH unit in CCRS
l_{RS2}	Horizontal rod length connecting the re-entrant angles of the outer RH unit in CCRS
l_{RS3}	Diagonal rod length of the inner SH unit in CCRS
l_{RS4}	Horizontal connecting rod length between inner SH and outer RH in CCRS
l_{RS5}	Vertical connecting rod length between inner SH and outer RH in CCRS
θ_R	Re-entrant angle of the RH
θ_S	Re-entrant angle of the SH
θ_{RS1}	Re-entrant angle of the outer RH unit in CCRS
θ_{RS2}	Re-entrant angle of the inner SH unit in CCRS
h_R	Height of the RH unit cell
h_S	Height of the SH unit cell
h_{RS}	Height of the CCRS unit cell
L_R	Horizontal length of the RH unit cell
L_S	Horizontal length of the SH unit cell
L_{RS}	Horizontal length of the CCRS unit cell
L_{R0}	Initial clamping length of the RH tensile sample
L_{S0}	Initial clamping length of the SH tensile sample
L_{RS0}	Initial clamping length of the CCRS tensile sample
t_R	Rod width of the RH
t_S	Rod width of the SH
t_{RS}	Rod width of the CCRS
δ_R	Thickness of the RH sample
δ_S	Thickness of the SH sample
δ_{RS}	Thickness of the CCRS sample

δ	Thickness of the sample
S	Scale factor (ratio of scaled size to original size)
ε_y	Transverse (lateral) strain
ε_x	Longitudinal (axial) strain
ν_{nom}	Nominal Poisson's ratio
ν_{ins}	Instantaneous Poisson's ratio
W	Total work during tensile loading
W_e	Elastic recovery work during unloading
e_W	Work recovery coefficient

S2. Geometric derivations of unit cells

When a tensile load is applied along the X-axis, stress is transferred through the connecting rods l_{RS4} and l_{RS5} to both the star-shaped and re-entrant hexagonal elements. In the first stable deformation stage, the external RH transforms from a re-entrant hexagon into a rectangular configuration, while the diagonal rods of the internal star-shaped structure rotate toward a near-vertical orientation, leading to pronounced expansion in the Y direction. In the second stable stage, the RH further evolves toward a regular hexagon, accompanied by the internal SH rods gradually aligning horizontally along the X direction and bulging outward along the Y direction. This coordinated and hierarchical deformation enables sustained axial stretching together with lateral expansion, resulting in a stable deformation mode of the CCRS over a large strain range.

Based on geometric relationships, the height h_{RS} of the CCRS unit cell is given by

$$h_{RS} = 2l_{RS1}\sin\theta_{RS1} \quad (1)$$

The horizontal length L_{RS} of an CCRS unit cell can be expressed in terms of l_{RS}, l_{RS1} and l_{RS2},

$$L_{RS} = 2(l_{RS2} - l_{RS1}\cos\theta_{RS1}) + l_{RS} \quad (2)$$

In addition, to evaluate the mechanical performance of the proposed CCRS structure, its two constituent structures, namely the RH and the SH, were employed for comparison. The corresponding unit cell structure and parameter schematics are shown in Figures 1(b)-ii and iii, respectively.

Based on geometric relationships of the unit cell in Figures 1(b)-ii, the total height h_R is related to the diagonal rod length l_{R1} and the concavity angle θ_R as follows:

$$h_R = 2l_{R1}\sin\theta_R \quad (3)$$

The horizontal length L_R of the RH unit cell is determined by the geometric parameters l_R, l_{R1}, and l_{R2}, and can be written as

$$L_R = 2(l_{R2} - l_{R1}\cos\theta_R) + l_R \quad (4)$$

Wherein, l_R, l_{R1} and l_{R2} denote the lengths of the horizontal short side, the diagonal rod, and the horizontal rod connecting the re-entrant angle, respectively. The unit of length is

millimeters (mm), and angles are expressed in degrees (°).

Similarly, from Figures 1(b)-iii, the total height h_S of the SH unit cell can be expressed as

$$h_S = 2\left(l_{S2} + \sqrt{2} l_{S1} \sin \theta_S/2\right) \quad (5)$$

Here, l_{S1} denotes rod length of the star-shaped structure, l_{S2} and l_{S3} are the lengths of the horizontal rods connecting the re-entrant angles, and $\theta_S$is the diagonal angle of the star-shaped structure. Because the unit cell is designed with a near-square layout, the horizontal and vertical lengths are equal, i.e., $L_S = h_S$.

S3. Fabrication Procedure of NPR Metamaterials

The NPR metamaterial samples were fabricated by casting silicone rubber into predesigned molds. The molds corresponding to the CCRS, RH, and SH unit cells were fabricated using 3D printing technology. Firstly, Ecoflex 00-30 silicone rubber (Smooth-On, Inc., USA) was prepared by mixing Part A and Part B at a mass ratio of 1:1. The mixture was then stirred at 250 rpm by the magnetic stirrer until homogeneous. After stirring, it was kept standing to remove air bubbles. Subsequently, the mixture was slowly poured into the molds and a glass slide was used to scrape off the excess, ensuring a flat surface. Finally, the completely cured silicone was demolded to obtain the three structural samples. All samples were placed in a 40°C oven for 2-3 hours to further enhance the mechanical properties and stability. Following the above procedure, the three NPR structures—CCRS, RH, and SH, were successfully fabricated.

The main equipment and key fabrication parameters used for preparing the 3D-printed molds are summarized in Table S2, providing a detailed reference to ensure reproducibility and consistency across all samples.

Table S2. Main equipment and key fabrication parameters for 3D-printed molds

Project	Parameters/Specifications
3D printer	Bambu Lab H2D
Construction materials	Polylactic acid (PLA)
Nozzle diameter	0.2 mm
printing speed	80 mm/s

Note: All molds were printed using unified slicing parameters and identical printing settings to ensure geometric consistency among samples.

S4. Cyclic loading testing

To prove the mechanical stability and long-term damage resistance ability of the CCRS, cyclic loading tests were conducted on the CCRS and its constituent structures at strain levels of 80%, 100%, 150%, and 180%, respectively. Both the loading and unloading speeds were set to 150 mm/min. Furthermore, the work recovery coefficient (e_W) was utilized to quantitatively characterize the recovery performance. The calculation formula is:

$$e_W(\%) = (W_e/W) \times 100\% \quad (6)$$

Where W represents the total work, defined as the area enclosed by the tensile loading curve and the tensile strain axis, whereas W_e represents the elastic recovery work, which is calculated as the area enclosed by the unloading recovery curve and the tensile strain axis.

S5. Definition and Measurement of Poisson's Ratio

In this study, Poisson's ratio is defined based on the contour changes observed during deformation of the CCRS structure. Specifically, the tensile process was continuously recorded via a camera, and image were extracted at certain time intervals (one frame per second).

From each image, the sample length L and outer contour width W were measured using ImageJ software. Based on these overall dimensional changes relative to the undeformed state, the Poisson's ratio value can be obtained by:

$$\nu_{nom} = -\frac{\varepsilon_y}{\varepsilon_x} = -\frac{(\Delta W/W_0)}{(\Delta L/L_0)} \quad (7)$$

where ε_y represents the nominal transverse strain and ε_x represents the nominal longitudinal strain. And, $\Delta L = L - L_0$, $\Delta W = W - W_0$ denote the changes in the overall sample gauge length and width, respectively. L_0 and W_0 are the initial dimensions in the undeformed state.

Generally speaking, the instantaneous Poisson's ratio ν_{inst} is defined as

$$\nu_{ins} = -\frac{d\varepsilon_y}{d\varepsilon_x} \quad (8)$$

which can be calculated from differential of the $\varepsilon_y - \varepsilon_x$ curve. It can be seen that the ν_{ins} indicates the geometrical variation relative to the previous state, while the ν_{nom} describes that with respect to the initial specimen dimensions.

To compare the two definitions under large deformation, Fig. S1 has been added in the Supporting Information. The figure presents both nominal and instantaneous Poisson's ratios of the CCRS structure over the entire strain range. The two curves follow nearly the same trend and remain close to each other throughout the deformation process.

(i) Under the small strain conditions, deformation is mainly caused by the rotation of the internal SH units, which leads to lateral expansion. In this range, the structural change is limited, and the nominal and instantaneous Poisson's ratios are nearly identical. Therefore, both definitions describe the auxetic response in a consistent manner.

(ii) Under large strain conditions (above 70%), the overall trend is that the absolute value of the Poisson's ratio gradually decreases. As shown in Fig. S1, both the nominal and instantaneous Poisson's ratio curves exhibit a gradual reduction in magnitude in this strain range. Although the structure still expands laterally, the increase in length caused by stretching becomes larger than the increase in width caused by rotation. In other words, the longitudinal strain grows faster than the transverse strain, which leads to a reduction in the magnitude of the negative Poisson's ratio. This change is related to the deformation mechanism at high strain.

As the strain increases, the rotation of the SH units gradually approaches its geometric limit. At the same time, the RH units take on more load, and the ribs begin to deform mainly by axial stretching. In this stage, additional deformation mainly contributes to elongation in the loading direction, while the ability of the structure to further expand in the transverse direction becomes limited. Because the longitudinal increase is greater than the transverse increase, the negative Poisson's ratio effect becomes weaker. Under large deformation, the instantaneous Poisson's ratio may show small local changes due to incremental geometric adjustments. These local fluctuations can also be observed in Fig. S1, but the overall trend remains close to that of the nominal Poisson's ratio. The difference between the two definitions remains small in the studied strain range. For this reason, the nominal Poisson's ratio is used to describe the overall auxetic behavior of the structure under both small and large strains.

In summary, the nominal Poisson's ratio is used to describe the overall geometric response of the CCRS structure under both small and large strains. At large deformation, the reduction in the magnitude of the negative Poisson's ratio is mainly related to the change in deformation mode, where longitudinal elongation becomes more dominant than lateral expansion, and the increase in length exceeds the increase in width.

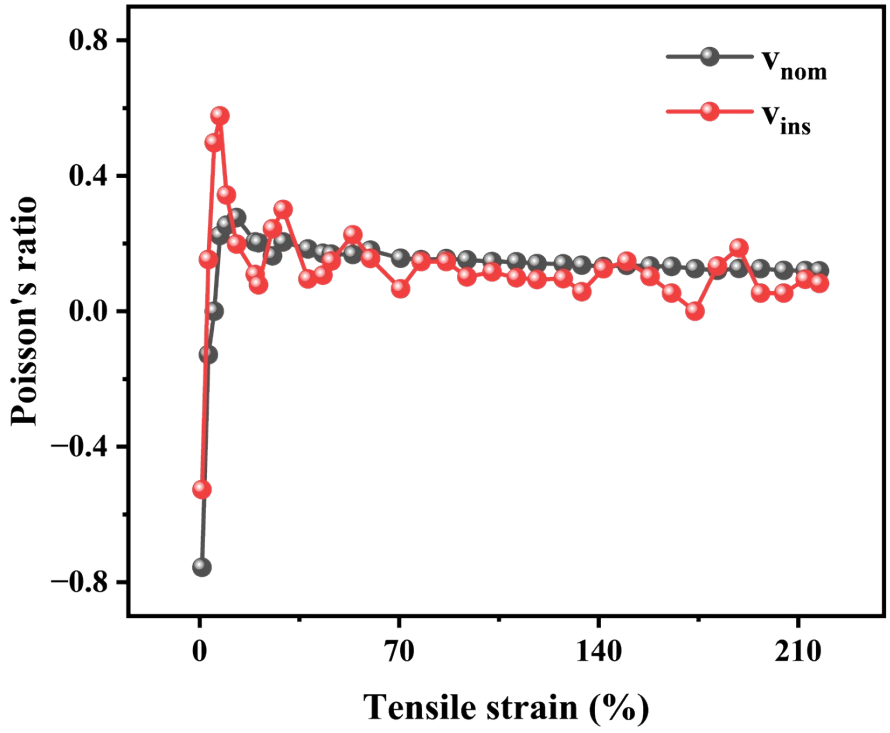

Fig.S1. Comparison of nominal and instantaneous Poisson's ratios of the CCRS structure under tensile loading.

S6. Deformation mechanisms of RH and SH structures

The deformation process of the RH and SH structures can both be divided into two stages, mainly governed by the rotation and bending of their respective rods (l_{R1}, l_{R2} for RH, l_{S1}, l_{S2} for SH) along with the increase of the re-entrant angle (θ_R for RH, θ_S for SH), yielding a lateral expansion, that is, the auxetic effect. Specifically, under the low strain range below 10%, the geometry of the RH structure gradually transforms from the initial re-entrant configuration toward a more open, quasi-rectangular configuration. This geometric opening facilitates rod rotation and bending, thereby accommodating axial deformation while promoting transverse expansion. In contrast, the SH structure deforms predominantly through a progressive increase in the diagonal angle θ_S, which gradually drives the unit cell toward a rectangular-like configuration. These low-strain behaviors are the main sources of the superior deformation characteristics compared with traditional structures and are confirmed by the corresponding experimental observations. As the tensile strain further increases, the re-entrant rods of RH and the diagonal rods of SH continue to rotate, and both structures gradually transform into a regular hexagon until structural failure occurs.

S7. Definition and Calculation of the Effective Tangent Modulus and initial Modulus

1) Definition of Effective Tangent Modulus:

In this study, the effective tangent modulus is defined as the slope obtained by linear fitting of the stress–strain curve within a given deformation stage. The stress-strain curves of the CCRS, RH, and SH structures are nonlinear under large deformation, and the slope changes continuously. Therefore, for each stage, a linear fit is applied over the corresponding strain range, and the fitted slope is used to describe the average stiffness of the structure in that stage. This fitted slope is defined as the effective tangent modulus. The effective tangent modulus describes how much additional stress is required to produce additional strain within a given stage. A larger value means that more stress is needed to further deform the structure, which indicates higher stiffness during that stage.

The effective tangent modulus values of the CCRS, RH, and SH structures at each deformation stage are summarized in Table S3. It can be seen that the effective tangent modulus of the CCRS structure is consistently higher than that of the RH and SH structures in all corresponding stages. This indicates that the collaborative deformation between the RH and SH units in CCRS leads to enhanced stiffness and improved mechanical performance compared with the single unit structures.

Table S3 Effective tangent modulus of CCRS, RH and SH at different deformation stage

Sage	CCRS (10^{-5}MPa)	RH (10^{-5}MPa)	SH (10^{-5}MPa)
I	3.06	0.956	1.08
II	6.44	2.06	1.89
III	9.88	3.69	3.37

2) Definition and Calculation of the initial Modulus:

In this study, the initial modulus refers to the average stiffness of the structure from the undeformed state to the yield point. It is calculated as the ratio of the yield stress to the yield strain. The procedure used to determine the yield point and calculate this modulus is described below.

Yield-stage modulus: The yield point is identified using the Meredith method [41], which is widely adopted for determining yield behavior in cellular materials. The procedure is as follows:

a) Draw a line connecting the origin (O) and the fracture point (A).

b) Draw a line parallel to OA that is tangent to the stress-strain curve; the tangent point (Y) is defined as the yield point.

c) Read the yield stress σ_Y and yield strain ε_Y at point Y.

d) The effective tangent modulus at the yield stage is then calculated as $E_{yield} = \sigma_Y / \varepsilon_Y$, representing the average stiffness from the undeformed state to yielding.

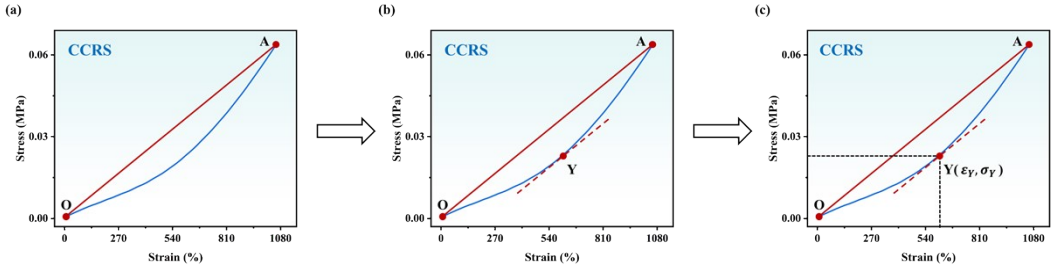

Fig.S2. Schematic illustration of the procedure used to determine the yield point and the effective tangent modulus based on the Meredith method. (a) Original engineering stress–strain curve of the CCRS structure, showing the undeformed state (O) and the fracture point (A). (b) Construction of a straight line OA connecting the origin and the fracture point, and a parallel line drawn to be tangent to the stress–strain curve; the tangency point Y is identified as the yield point. (c) Determination of the effective tangent (secant) modulus at the yield stage, calculated as $E_{yield} = \sigma_Y/\varepsilon_Y$, corresponding to the slope of the line OY and representing the average stiffness from the undeformed state to yielding.

Ref [41]: R. Meredith, Journal of the Textile Institute Transactions, 1954, **45**, T30-T43.

S8. Statistical validation of tensile performance of CCRS, RH, and SH structures

For each structure (CCRS, RH, and SH), three repeat experiments were tested under identical tensile conditions. To demonstrate repeatability, three representative stress-strain curves from each structure are presented in Fig. S3(a). As shown in the figure, the three curves corresponding to each structure almost completely overlap over the entire deformation range, indicating excellent consistency and minimal specimen-to-specimen variation. This overlap confirms the robustness and reproducibility of the tensile response.

Furthermore, the maximum tensile strain and maximum tensile stress were statistically analyzed based on three specimens for each structure. The mean values and standard deviations are summarized in Table S4, and the corresponding comparison with error bars is shown in Fig. S3(b). The relatively small standard deviations compared with the mean values indicate limited data dispersion and good experimental stability.

Overall, the results demonstrate high repeatability and experimental reliability, with minimal variation among specimens and consistent tensile performance across all structures.

Table S4 Statistical mechanical performance of CCRS, RH, and SH structures

Sample	Maximum tensile strain (*10³ %)	CV (%)	Maximum stress (MPa)	CV (%)
CCRS	1.22	4.874	0.12	8.957
RH	1.82	4.203	0.09	10.578
SH	1.24	8.738	0.05	6.857

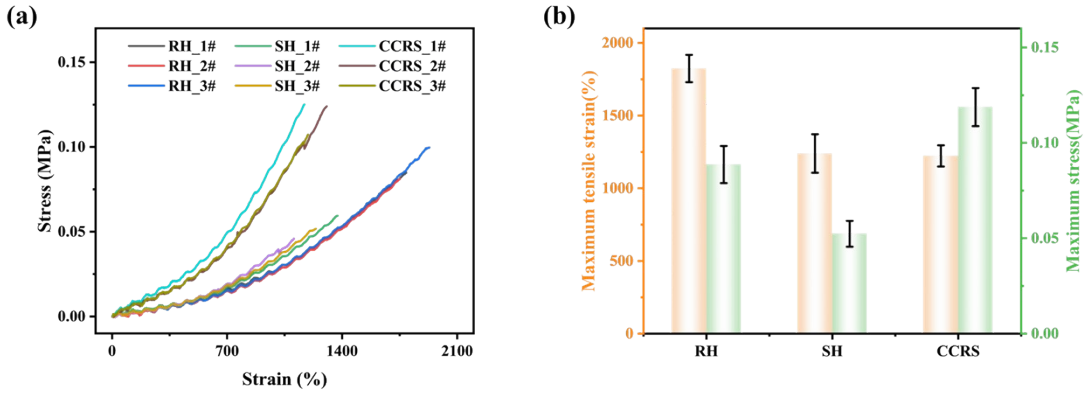

Fig.S3. Statistical validation of tensile performance. (a) Representative engineering stress–strain curves of CCRS, RH, and SH structures. Three independent specimens are shown for each structure. (b) Comparison of maximum tensile strain and maximum tensile stress of CCRS, RH, and SH structures with error bars representing standard deviations (n = 5).